HHS Public Access

Author manuscript

Langmuir. Author manuscript; available in PMC 2016 May 13.

Published in final edited form as:

Langmuir. 2015 December 1; 31(47): 12993–13002. doi:10.1021/acs.langmuir.5b03177.

Highly Compliant Vascular Grafts with Gelatin-Sheathed Coaxially Structured Nanofibers

Naveen Nagiah, **Richard Johnson**, **Roy Anderson**, **Winston Elliott**, and **Wei Tan***

Department of Mechanical Engineering, University of Colorado at Boulder, Boulder, Colorado 80309, United States

Abstract

We have developed three types of materials composed of polyurethane–gelatin, polycaprolactone–gelatin, or polylactic acid–gelatin nanofibers by coaxially electro-spinning the hydrophobic core and gelatin sheath with a ratio of 1:5 at fixed concentrations. Results from attenuated total reflection-Fourier transformed infrared spectroscopy demonstrated the gelatin coating around nanofibers in all of the materials. Transmission electron microscopy images further displayed the core–sheath structures showing the core-to-sheath thickness ratio varied greatly with the highest ratio found in polyurethane-gelatin nanofibers. Scanning electron microscopy images revealed similar, uniform fibrous structures in all of the materials, which changed with genipin cross-linking due to interfiber interactions. Thermal analyses revealed varied interactions between the hydrophilic sheath and hydrophobic core among the three materials, which likely caused different core–sheath structures, and thus physicomechanical properties. The addition of gelatin around the hydrophobic polymer and their interactions led to the formation of graft scaffolds with tissue-like viscoelasticity, high compliance, excellent swelling capability, and absence of water permeability while maintaining competent tensile modulus, burst pressure, and suture retention. The hydrogel-like characteristics are advantageous for vascular grafting use, because of the capability of bypassing preclotting prior to implantation, retaining vascular fluid volume, and facilitating molecular transport across the graft wall, as shown by coculturing vascular cells sandwiched over a thick-wall scaffold. Varied core–sheath interactions within scaffolding nanofibers led to differences in graft functional properties such as water swelling ratio, compliance, and supporting growth of cocultured vascular cells. The PCL–gelatin scaffold with thick gelatin-sheathed nanofibers demonstrated a more compliant structure, elastic mechanics, and high water swelling property. Our results demonstrate a feasible approach to produce new hybrid, biodegradable nanofibrous scaffold biomaterials with interactive core–sheath structure, good biocompatibility, and tissue-like viscoelasticity, which may reduce potential problems with the use of individual polymers for vascular grafts.

Graphical abstract

*Corresponding Author. wei.tan-1@colorado.edu.

The authors declare no competing financial interest.

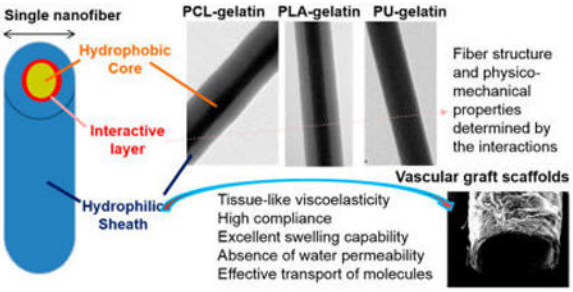

1. INTRODUCTION

Vascular disease is one of the leading causes of morbidity and mortality in developed countries, and thereby necessitates the replacement of diseased artery or vein through surgical intervention.[1,2] Tissue engineering offers an alternative approach of designing biomaterials for small diameter artery regeneration.[1] A typical tissue-engineering scaffold for artery grafting must enable the adhesion and proliferation of endothelial cells and smooth muscle cells leading to the deposition of extracellular matrix (ECM) proteins and withstand physiological hemodynamic pressures.[3] Of the various methods used for mimicking the structure and function of the tissue ECM, electrospinning has proven to be a facile method for generating micro- and nanofibers from a variety of materials that include biodegradable polymers. In electrospinning, polymer fibers are generated when an electrified jet of polymer solutions is continuously stretched due to the electrostatic repulsions between the surface charges and the evaporation of solvent.[4] The high ratio of the surface area to volume or to the mass of these fibers is highly advantageous in biomedical applications such as tissue engineering and drug delivery.[5–8]

The use of a mixture of hydrophobic and hydrophilic polymers or a mixture of natural and synthetic polymers has been attempted in the past for synthesis of tissue-engineering scaffolds.[9,10] However, using conventional methods such as blending fibers or layering materials, the adhesion and interaction between the blended systems were often too low to obtain a mechanically stable scaffold while providing desired pore size and porosity. Coaxial electrospinning provides a unique approach to construct a structured polymer blend, wherein the polymers are highly interactive at the nanoscale to bring about novel properties. Coaxially electrospun fibers in comparison with coated or blended fibers have shown enhanced biocompatible and mechanical properties for tissue engineering and regenerative applications.[11,12] Few attempts have been made using coaxial electrospinning to develop small diameter artery grafts.[13–17] In coaxial electrospinning, two compartments containing either different polymer solutions or a mixture of a polymer solution for the formation of shell and a nonpolymeric Newtonian liquid or even a powder for the formation of core are used to initiate a core–shell jet. With the core–shell jet solidifying, core–shell fibers are deposited on a grounded electrode.[5] Under most fabrication conditions, the shell fluid is able to be processed with electrospinning, while the core fluid is not electrospinnable.[18]

Biocompatible and biodegradable hydrophobic polymers like polycaprolactone (PCL), polyurethane (PU), and polylactic acid (PLA) have been used in myriad tissue engineering

applications including vascular regeneration.[19–21] In spite of the high mechanical stability of these polymers, they lack the innate reactive sites for cell adhesion. The hydrophobic nature of PCL, PU, and PLA also tends to attract platelet and plasma protein adhesion, leading to the aggregation and intimal hyperplasia of the artificial blood vessels.[22] Collagen is one of the most predominant ECM proteins found in the vasculature. However, electrospinning with the use of strong organic solvents always causes the denaturation of collagen into gelatin.[23] Gelatin possesses competent biodegradable properties along with excellent biocompatibility and nonantigenicity comparable to collagen.[24,25] The combination of hydrophobic polymer and gelatin may provide appropriate graft strength, compliance, and viscoelasticity. This study attempts to coaxially electrospin three different types of vascular grafts composed of nonantigenic hydrophilic gelatin sheathing with the hydrophobic core made of PU, PCL, or PLA, which forms fibrous scaffolds for potential small diameter (<6 mm in diameter) vascular grafts. The hydrophobic core provides the mechanical strength and stability of the scaffold, while the gelatin sheath ensures its enhanced biocompatibility and mimetic viscoelasticity. The physical, mechanical, and biological performances of the hybrid nanofibrous scaffolds are evaluated here.

2. EXPERIMENTAL: MATERIALS AND METHODS

2.1. Materials

All polymers and chemicals were purchased from Sigma-Aldrich Inc. (St Louis, MO) unless specified otherwise.

2.2. Electrospinning of Polymer Fibers

The apparatus used for obtaining coaxial fibers was developed in house. Core hydrophobic polymer solution was passed through the inner needle of 22 G (0.71 mm in internal diameter), and the sheath gelatin solution was passed through the outer needle of 16 G (1.65 mm in internal diameter). A dual syringe holder was used to place the syringes loaded with polymer solutions. This design allows the solutions to be extruded simultaneously. Polymer solutions of 1 wt % concentration of PU, PCL, or PLA and 5 wt % gelatin were prepared by dissolving a predetermined amount of PU, PLA, or PCL and gelatin in 1,1,1,3,3,3 hexafluoro-2-propanaol (HFP). The solutions obtained after stirring for 6–8 h were loaded in 5 mL syringes connected to the positive terminal of a high voltage ES30P 10 W power supply (Gamma High Voltage Research, Ormond Beach, FL). The polymer solutions were extruded at 1 mL/h using syringe pumps (Pump 11 Plus, Harvard Apparatus, Boston, MA) and subjected to an electric potential of 1 kV/cm. The fibers were deposited onto a grounded static aluminum substrate or cylindrical aluminum rod of 5 mm in diameter rotating at 150 rpm and placed at a distance of 10 cm perpendicular to the needle. The aluminum rod was coupled to a BMU230AP-A-3 brushless DC motor (Oriental Motor Corp, USA). The obtained samples were stored at room temperature until further use.

2.3. Cross-Linking of Electrospun Fibers

The scaffolds composed of coaxially electrospun fibers were subjected to cross-linking for 48 h by immersion in solution containing 0.25% (w/v) genipin dissolved in 100% ethanol.

Immediately after the cross-linking process, fibrous scaffolds were rinsed with phosphate buffered saline (pH 7.4) and used as such or air-dried overnight.

2.4. Material Characterizations

2.4.1. Scanning Electron Microscopy—The aluminum substrates coated with the electrospun fibers were mounted on brass stubs and observed under a scanning electron microscope (JEOL JSM 6480 LV, USA) operating at an accelerating voltage of 5–20 kV. The diameters of about 50 different fibers were measured in each of the cases using the UTHSCA Image tool to obtain their average diameter.

2.4.2. Transmission Electron Spectroscopy—The nanostructure of the coaxial fibers was observed using an H7650 transmission electron microscope (Hitachi Ltd., Tokyo, Japan) operated at 80 kV. The electrospun nanofiber samples for TEM observation were prepared by directly depositing the as-spun fibers on carbon-coated TEM grids.

2.4.3. ATR-FTIR Spectroscopy—Attenuated total reflection-Fourier transform infrared spectroscopy (ATR-FTIR) measurements were carried out on peeled fibrous membranes using a Nicolet 6700 FTIR spectrometer (Thermo Fisher Scientific, USA) equipped with a diamond ATR crystal. Typically, 30 scans were signal-averaged to reduce spectral noise. The spectrum of the samples was recorded from 600 to 4000 cm^{-1}.

2.4.4. Thermal Analysis—Thermogravimetric Analysis, Differential Thermal Analysis, and Differential Scanning Calorimetry Analysis—Thermogravimetric analysis (TGA) of the fibers was performed using a universal Netzsch 204 F1 instrument (Phoenix, AZ). About 5 mg of the samples was heated at 10 °C min^{-1} in a temperature range of 0–600 °C using platinum crucibles. Differential thermal curves were obtained from the TGA curves by plotting a graph between derivative weight % and temperature.

Differential scanning calorimetry (DSC) analysis of the fibers was performed from 0 to 300 °C at 20 °C min^{-1} using a Netzsch 204 F1 instrument (Phoenix, AZ). The instrument was calibrated using an indium standard, and the calorimeter cell was flushed with liquid nitrogen at 20 mL min^{-1}.

2.4.5. Tensile Strength Measurement—Samples of electrospun nanofibrous membranes with dimensions of 100 mm × 5 mm were tested for their tensile strength. Load–elongation measurement was carried out at a crosshead speed of 5 mm/min, 25 °C temperature, and relative humidity of 65%. The percentage of elongation at break (%) was measured using a universal testing machine (INSTRON model 1405, Shakopee, MN), at an extension rate of 5 mm/min.

2.4.6. Rheometry Testing—The viscoelastic properties of coaxial scaffolds were investigated under shear deformation using the ARES or ARG2 rheometer (TA Instrument, New Castle, DE). The ARES is designed to measure the expended torque. Samples were analyzed on ARES using the plate geometry (diameter = 8–10 mm; gap set between 0.25 and 0.5 mm). Strain sweep measurements spanning from 0.1 to 50% strain were conducted at 10 points each decade of strain (e.g., 0.1–1%). Frequency sweeps were conducted at a

stress–strain range of constant oscillation frequency. Oscillatory frequency sweep tests were conducted with logarithmic step increases between 0.1 and 50 Hz to identify the linear region for all scaffolds. The storage modulus (G') and loss modulus (G'') of scaffolds as well as tan δ (tan $\delta = G'/G''$) were determined in the linear viscoelastic region (LVR). Using G' and G'', the complex storage modulus (G^*) can be calculated using $G^* = G' + iG''$. Shear stress was determined in response to constant strain application, reflecting the difference in material viscosity. In order to avoid sample slipping during rheometry measurement, the glass slides were treated for sample attachment. Briefly, slides are immersed in 20% sulfuric acid for ~30 min and then washed in deionized water three times changing the water at 5 min intervals. Subsequently, the slides were immersed in acetone for 30 min and then in aminopropyltriethoxysilane overnight. Then, the slides were washed in acetone three times, followed by three washes in deionized water. Lastly, the slides were immersed in 2.5% glutaraldehyde for 1 h followed by two washes in deionized water, before they were used to collect nanofibers for rheometry measurements.

2.4.7. Swelling and Water Retention Capacity of Coaxially Electrospun Fibers

—The electrospun samples were placed in deionized water for a period of 72 h. The samples were then removed, centrifuged for 15 min at 1500 rpm (Eppendorf Centrifuge 5415D, Hauppauge, NY), and weighed. Water retention capacity was determined with the increase in the weight of the fibers through the following equation

$$\text{Water retention } (\%) = \left(\frac{w - w_{\mathrm{d}}}{w_{\mathrm{d}}}\right) \times 100\%$$

where w is the weight of each specimen after submersion for a certain period of time and w_{d} is the weight of the specimen in its dry state before submersion.

2.5. Vascular Graft Functional Characterizations

The water permeability, burst strength, compliance, and suture retention strength of vascular grafts were determined according to the methods prescribed in the industrial standard—ANSI/AAMI/ISO 7198:1998/2001/(R) 2004 (Cardiovascular Implants: Tubular Vascular Prostheses). A custom-made apparatus designed for determination of water permeability, burst pressure, and compliance was used.

2.5.1. Water Permeability—Tube adapters were inserted onto both ends of the multilayer graft. Paraffin films were used to secure the graft on the adapters. Then, the graft was cannulated by connecting one end of the graft to a water reservoir with a flow valve and the other end was connected to the other end of the water reservoir. Water pressurized at 16 kPa (120 mmHg) was imposed using a pulsatile flow pump. Once the flow became steady, the permeated fluid through the graft due to the pressure was collected in a beaker and the water volume collected within 1 min was measured. The graft permeability (units: mL/cm^2/ min^{-1}) was determined using the equation

$$S = Q/A$$

where S is the graft permeability, Q is the fluid volume passing through the graft, and A is the cross-sectional area of the aperture in the sample holder.

2.5.2. Burst Strength—Tube adapters were inserted on both ends of the vascular grafts. Paraffin films were used to secure the graft onto the latex tube near the adapters. The graft was then loaded onto a custommade fixture and connected to a flow network via pressure gauges on both ends of the graft. Water was pressurized through the graft at increments of 10 mmHg. The increasing pressure led to an expansion of the graft diameter and surface area. The expansion was allowed until graft failure occurred. The pressure at which this failure of the vascular graft occurred was recorded as the burst strength or burst pressure of the graft.

2.5.3. Compliance—Compliance was measured by a similar method adopted for burst pressure. A tubular graft was cannulated with a latex tube inserted in a way similar to the burst strength test. The graft was then loaded onto a custom-made fixture and connected to a flow network via pressure gauges on both ends of the graft. The pressure in the graft was controlled using varying speed of a water pump, to obtain a steady pressure from 10 to 200 mmHg, with an increment of 10 mmHg. At each pressure, images of the graft dilatation were taken using a camera (Canon EOS 450D, Japan). These images were analyzed using a customized script in MatlabVR (MathWorks, USA) to obtain the graft diameter at each pressure point. Compliance was measured using the equation

$$C=[(R2-R1)/R1]/(P2-P1)\times 10^4$$

where C is % of compliance, $R1$ is the original graft diameter, $R2$ is the changed graft diameter, $P1$ is the inlet pressure, and $P2$ is the outlet pressure.

2.5.4. Suture Retention—Suture retention was measured by cutting the 3D vascular graft into rectangular strips with dimensions of 10 mm × 5 mm. A suture was inserted 2 mm from the end of the stretched strip of the graft through the graft wall to form a half loop, and the other end of the graft was attached to the lower clamp of the tensile testing system. The other end of the suture was attached to a 2 kN load cell. The suture was pulled at a rate of 10 mm/min. The force required to rupture the graft wall was recorded as suture retention.

2.6. Biocompatibility of the Electrospun Fibers in Vitro Biocompatibility by MTT Assay

Human pulmonary artery endothelial cells (hECs) from Lonza Inc. (Basel, Switzerland) were cultured on the luminal (top) surface of a coaxial electrospun fibrous mat at a seeding density of 1×10^5 cells/cm^2 at 37 °C with 5% CO_2, 95% air and complete humidity for 72 h. Human pulmonary artery smooth muscle cells (hSMCs) were then seeded on the back (bottom) side of the scaffolds with hECs at a seeding density of 5×10^4 cells/cm^2 for 72 h. The cell culture medium was composed of DMEM with 10% FBS, 4 mL of 1 mM VEGF and supplemented with an antibiotic cocktail of penicillin (120 units per mL), streptomycin (75 mg/mL), gentamycin (160 mg/mL), and amphotericin B (3 mg/mL). After 6 days, the culture medium was replaced with a serum-free medium containing thioazolyl blue (MTT) and incubated for 4 h at 37 °C in a humidified atmosphere of 5% CO_2. The medium was

aspirated, and the formazan needles were dissolved in 500 μL of dimethyl sulfoxide. The absorbances of the solutions were read at 570 nm, and the results were expressed as means of three experiments. Data were statistically analyzed using ANOVA with a sample size of at least 3 ($n \geq 3$) for each set with $p < 0.05$ for statistical significance. To study cell morphology, the cell-seeded scaffolds were rinsed with PBS after 6 days of cell seeding and fixed using 10% neutral formalin buffer for 5 h at 4 °C and stained with DAPI and F-actin. The stained cells were examined with appropriate filters using a fluorescent microscope.

3. RESULTS AND DISCUSSION

3.1. Morphology of Coaxially Blended Electrospun Fibers

Parts A, B, and C of Figure 1 show the TEM images of gelatin-sheathed coaxial fibers with the core made of PCL, PLA, and PU, respectively. The fiber diameters of these three systems range between 150 and 400 nm. The core-to-sheath diameter ratio of the nanofibers was found to be lowest for the PCL–gelatin system and highest for the PU–gelatin system. Since the core-to-sheath concentration ratio was maintained at a ratio of 1:5 in all systems, the difference in the diameter ratio might be due to the difference in the viscosity of the core polymer solutions and/or the possible formation of an interactive core–sheath layer which is sandwiched between the pure hydrophobic core and the hydrophilic gelatin sheath. PCL, PU, and PLA are often electrospun using solvent(s) like chloroform and HFP, but when they are blended with natural polymers such as collagen, gelatin, and chitosan, strong acidic solvents like HFP or 2,2,2-trifluoroethanol should be used. These solvents have (i) a high electrical conductivity which assists electrospinning and (ii) a reduced surface tension in polymer solutions which enables the use of a lower concentration of polymers for electrospinning.[11] HFP was thus chosen to coaxially electrospin blends of PCL–gelatin, PLA–gelatin, and PU–gelatin.

Parts D, E, and F of Figure 1 respectively represent the SEM images of PCL–gelatin, PLA–gelatin, and PU–gelatin coaxial electrospun fibers. The average nanofiber diameter of all three systems is shown in Table 3. The average fiber diameter was found to be lowest in the case of the PU–gelatin system, while the highest fiber diameter was seen in the PCL–gelatin system. In order to observe the change in the morphology of the coaxial fibers after cross-linking, SEM imaging of genipin-cross-linked fibers was performed after the samples were dried. Images are exhibited in parts G, H, and I of Figure 1, respectively. An increase in fiber diameters was observed in addition to the coalescence of fibers at the junctions (as illustrated by arrows in Figure 1G–I). The coalescence of fibers was most pronounced in the case of the PU–gelatin system followed by the PLA–gelatin system and then the PCL–gelatin system. In the cases of the PCL–gelatin and PU–gelatin systems, areas of coalescence-caused pore occlusion in the fibrous structure (Figure 1H and I) were obvious. The occlusion was highest in the PCL–gelatin system. Cross-linking gelatin with genipin has been reported to have an effect on increasing the average fiber diameter.[26] Therefore, the changes found in the fiber networks of all the gelatin-sheathed hybrid systems after cross-linking were likely caused by cross-linking-induced changes in the interfiber and/or intrafiber interactions. In a coaxial system, the interaction among the gelatin fibers likely depends upon the thickness of the fiber coating or sheath diameter. As the thickness of the

sheath decreases, a higher degree of interaction between the fibers in close proximity more likely occurred as in the case of PU–gelatin. Hence, the core–sheath intrafiber interaction was more pronounced in the PCL–gelatin coaxial system, while the interfiber interaction was more predominant in the PU–gelatin coaxial system. The interfiber interactions might enhance the stability and mechanical integrity of the scaffold. Moreover, for vascular graft applications, the occlusion of porous structures at certain junctions might help to reduce the permeability of the scaffolds to the blood during the initial stages of implantation and vascular regeneration. Parts J, K, and L of Figure 1 respectively show representative SEM images of the 3D coaxial vascular grafts made of PCL–gelatin, PLA–gelatin, and PU–gelatin collected on a rotating aluminum mandrel of 5 mm in diameter. The diameter of all three coaxially electrospun vascular grafts was 5 mm, and the thickness of the grafts was in the range 0.5–0.6 mm.

3.2. ATR-FTIR Spectroscopy Results Demonstrating the Gelatin Coating of Coaxially Electrospun Fibers

The ATR-FTIR spectra of coaxially electrospun fibers and individual hydrophobic electrospun fibers are shown in Figure 2. The characteristic absorption band between 1700 and 1750 cm^{-1} in all individual hydrophobic polymers is mainly due to the ester carbonyl group (C═O). The peaks observed at 2943 and 2928 cm^{-1} of PCL and PU electrospun fibers correspond to C—H stretching bands of the CH_2 and CH_3 groups,[27–30] while the vibration due to O—C—O symmetric and asymmetric stretching, observed in the range 1226–1280 cm^{-1}, confirms the presence of the interactions among the electrospun fibers. Vastly different from the spectra of individual hydrophobic electrospun fibers, coaxially electrospun fibers show characteristic peaks only for gelatin, further confirming the coating of gelatin over PCL, PU, and PLA fibers. Gelatin on the coaxially electrospun fibers exhibited an amide I peak (C═O stretch) at 1636–1640 cm^{-1}, amide II peak (N—H bend and C—H stretch) at 1542–1548 cm^{-1}, amide III peak (C—N stretch plus N—H in phase bending) at 1240 cm^{-1}, and broad amide A peak (N—H stretching vibration) in the range 2900–3450 cm^{-1}.[31,32] In particular, the amide A peaks present are the distinguishing features of gelatin, indicating coaxially electrospun gelatin. In addition, a strong peak at 1445 cm^{-1} was observed due to the aldimine absorption. It was also found that the smooth amide II peak got converted into several small peaks.[31,32] The most common and prominent peaks are listed in Table 1. Since ATR-FTIR measures only the reflectance from a film surface, the degree of interaction between the core and sheath polymers could not be discerned.

3.3. Thermal Analysis Results of the Coaxially Electrospun Fibers

The thermal stability of the coaxially electrospun fiber systems was evaluated using TGA, differential thermal analysis (DTA), and DSC. The results are shown in Figure 3 and Table 2. DSC results show the different melting or glass transition temperatures of individual polymers and their coaxial blends (Figure 3A). The thermal stability of the coaxially blended polymeric vascular scaffolds was found to be sufficiently high for vascular tissue engineering applications. The transition temperature of gelatin was recorded to be at 105.3 °C, while the melting peaks of PLA and PCL were recorded at 187.3 and 58.1 °C, respectively. In the DSC results of coaxial blends, we found an occurrence of a single broad

peak in the cases of PU–gelatin and PLA–gelatin systems and two peaks in the case of PCL–gelatin system. The occurrence of a single broad peak in a blended system indicates the limited interaction between the two constituent polymers.[11] Another reason for the single peak formation might be due to the transfer of heat from gelatin to the core material. The increased pressure and temperature within the gelatin walls of the composite nanofibers might lead to melting of the core polymers at a lower temperature. In the case of the PCL–gelatin coaxial system, the first smaller peak falls between the melting and denaturation temperatures of PCL and gelatin, which is followed by a much broader peak with higher melting enthalpy than the other coaxial systems. Since PCL is well encapsulated within the gelatin layer, as demonstrated through our TEM and ATR-FTIR results, the smaller peak could be a shift in the denaturation temperature of gelatin to lower temperature due to the interaction between the polymers.

To further illuminate the core–sheath polymer interactions within the nanofibers of the three different systems, TGA and DTA were performed. The results (Figure 3B and C) showed that individual polymers with the exception of PU and gelatin were found to undergo a single-step weight loss while the coaxial counterparts underwent a two-step or three-step weight loss. It was found that the $T_{-5\%}$ values of coaxially electrospun fibers were vastly different from the individual polymers, falling between the $T_{-5\%}$ values of gelatin sheath and hydrophobic core polymers. The initial weight loss of gelatin occurs between 40 and 100 °C, which corresponds to the water loss in gelatin. Such water loss in coaxially electrospun systems was much lower when compared to gelatin, and constitutes only 1% of weight loss in the temperature range 40–100 °C. Different from gelatin, the individual hydrophobic core polymers did not undergo any degradation between 40 and 100 °C, indicating the absence of water molecules. After its initial weight loss, gelatin was found to be quite stable until the temperature reached 275 °C, which corresponded to the chain scission of ester linkages in gelatin, while the coaxially electrospun fibrous scaffolds underwent a rapid degradation at a higher temperature.[10] Further, a gradual degradation of gelatin occurred beyond 500 °C and corresponded to the breaking of amide and imide bonds in gelatin. Compared to gelatin and coaxially spun systems, the individual hydrophobic core polymers had endured a much higher thermal stability with an onset degradation temperature between 277 and 388 °C. PCL had the highest thermal stability followed by PU and PLA. PCL and PLA showed a single step weight loss between 329–484 °C and 268–422 °C, respectively, which could be attributed to the chain scission of ester linkages in both polymers.[33,34] PU underwent a two-step weight loss between 277–403 °C and 404–504 °C. The first step degradation was due to the scission or cleavage of C–O bonds in PU, and the second step degradation occurred due to the cleavage of C–N of diisocyanate bonds in PU.[35] The coaxially electrospun fibers of PU–gelatin and PCL–gelatin underwent a three-step weight loss, while coaxially electrospun PLA–gelatin underwent a two-step weight loss. The initial major weight loss for PU–gelatin and PCL–gelatin coaxial systems falls between 201 and 322 °C with $Tmax_1$ values of 249 and 271 °C, respectively. The second step weight loss occurred between 260 and 425 °C with $Tmax_2$ values of 352 and 376 °C, respectively. The final weight loss step occurred between 400 and 540 °C with $Tmax_3$ values of 433 and 471 °C, respectively. In the case of PLA–gelatin, the first step weight loss occurred between 150 and 254 °C with a $Tmax_1$ value of 232 °C and a second step weight loss between 267

and 453 °C with the $Tmax_2$ value at 352 °C. All coaxial systems exhibited a shift in the thermal peaks to lower temperatures due to the interaction of the hydrophobic polymers with gelatin. On the basis of the degree of interactions between the core and sheath polymers, a corresponding shift in the thermal peaks was observed. A schematic representation illustrating the type of interactions between the core and sheath polymers is shown in Figure 4. On the basis of the three-step weight loss in PU–gelatin and PCL–gelatin coaxial fibrous systems, the first step degradation may correspond to the noninteractive outermost sheath layer of gelatin cross-linked by genipin. The second step degradation indicates the degradation of the interactive layers of hydrophobic core and hydrophilic sheath layers. A distinct possibility of weak hydrogen interaction between the hydrophobic core and gelatin sheath could be the cause of the second degradation step. The third step of degradation corresponds to the noninteractive degradation of the hydrophobic core. Because the $Tmax_2$ value of the PLA–gelatin coaxial system was very close to the $Tmax_1$ value of pure PLA and tended to shift to lower temperatures after interaction, the degradation temperatures of the interactive layers and the noninteractive core may be overlapped to form a broader peak in the DTA result.

3.4. Water Permeability and Swelling Properties

The physicomechanical properties of the three-dimensional (3D) tubular vascular grafts were evaluated through standard tests for tubular cardiovascular implants in medical industries, including testing the water permeability, burst strength, compliance, and suture retention. The water permeability of all the designed coaxially electrospun vascular grafts was found to be 0 $mL/cm^2/min$ at a constant pressure of 120 mmHg for 1 min. The water permeability values can be largely attributed to high water swelling properties of the coaxially electrospun grafts (Table 3), while the average swelling properties were found to be directly proportional to the sheath thickness of gelatin. The electrospun scaffolds made of coaxially structured PCL–gelatin nanofibers exhibiting the thickest gelatin sheath were found to have the highest swelling ratio of 202%, while the scaffolds made of coaxially structured PU–gelatin nanofibers exhibiting the thinnest gelatin sheath showed the lowest swelling ratio of 94%. These swelling and water permeability behaviors indicate that the tubular scaffolds made of coaxially structured hybrid nanofibers function like hydrogel materials in an aqueous environment. As the flow of water went through the tubular graft scaffolds, the immediate swelling of the fibrous scaffold could lead to an occlusion of pores. The partial occlusion of pores in the fibrous matrix, established after cross-linking, also partially accounted for reduced water permeability of the tubular scaffolds. Moreover, the deposition of 15–20 layers of nanofibers on the rotating cylindrical aluminum rod with a surface area of approximately 20 cm^2, forming small water channels with high tortuosity, could also concur to reduced porosity of the tubular scaffold.

The absence of water permeability may be beneficial for using these tubular scaffolds as vascular grafts by skipping the preclotting procedure before implantation.[36] The preclotting step is necessary for almost all the existing vascular grafts made of hydrophobic materials such as PTFE, PCL, or PLA. Also, for those existing hydrophobic grafts, it is suggested that the water permeability values lower than 600 $mL/cm^2/min$ could have a low healing rate due to limited transport of nutrient and other signaling molecules through the graft wall.[36,37]

With hydrogel-like characteristics, vascular scaffolds made from coaxially structured nanofibers are not only capable of bypassing preclotting and retaining the overall vascular fluid volume but also capable of having the advantage of containing high water content to facilitate molecular transport. The presence of gelatin with high water retention ensures a continuous molecular transport through diffusion. Moreover, gelatin has a short half-life *in vivo*; thus, the occlusion of pores in these gelatin-sheathed coaxially designed scaffolds may recede within a short time period, when cells are capable of depositing their own matrix materials.[11]

3.5. Mechanical Properties (i.e., Tensile Property, Viscoelastic Property, and Suture Retention) of the 3D Vascular Scaffolds with Coaxially Spun Nanofibers

The average tensile modulus and suture retention as well as dynamic modulus (G' and G'') of the coaxially blended nanofibrous vascular grafts are listed in Table 3. Results show PCL–gelatin has the highest suture retention with a peak load of approximately 4 N and PU–gelatin has the lowest value. The suture retention values are comparable to the native vessels like saphenous veins and should be eligible for graft implantation.[35–37] Stress and strain values as well as the Young's modulus of the graft scaffolds were calculated on the basis of the load–extension curves. Figure 5A illustrates the representative stress–strain curves. Compared to PCL–gelatin and PLA–gelatin scaffolds, both of which were highly elastic and showed failure in a plastic manner, the PU–gelatin scaffold was stiffer and failed in a more brittle manner. The tensile modulus of the scaffolds was found to be correlated with the difference in core diameter of the grafts, instead of that of the core materials.[33] PCL–gelatin scaffolds exhibited the lowest modulus value of 5.98 MPa, while PU–gelatin scaffolds showed the highest modulus of 70.01 MPa. Similarly, using rheometry, dynamic viscoelastic properties including the storage modulus (G'), the average complex modulus (G*), and shear stress values under the constant strain (reflecting viscosity values) were determined. The results followed the same trend as uniaxial tensile studies, showing the highest values for PU–gelatin and the lowest values for PCL–gelatin. Figure 5B shows the difference in complex modulus as a function of strain within the linear viscoelastic regions (LVR). In addition to the ratio of core and shell in the nanofibers, the interdiffusion and interaction of gelatin with core polymers during coaxial electrospinning may also contribute to the modulus or rigidity of the scaffolds. Overall, the addition and interaction of gelatin with the core hydrophobic polymer led to the formation of a graft with tissue-like viscoelasticity and elasticity. Additionally, rheometry tests in strain sweep (Figure 5C) showed a LVR for all three scaffolds. While the strain sweep illustrates similar dynamic mechanical responses among these scaffolds, the PLA–gelatin fibrous scaffolds displayed a longer LVR, indicating constant behavior at higher shearing strain when compared to the other two, which is desirable for a vascular graft. Frequency sweep (data not shown) also illustrates that the LVR was successfully found.

3.6. Burst Pressure of Tubular Vascular Scaffolds with Coaxially Structured Nanofibers

The average burst pressure values of the 3D vascular scaffolds with coaxially structured fibers are shown in Table 3. It was found that the burst pressure values were inversely proportional to the sheath thickness. The average burst pressures of the vascular scaffolds with PCL–gelatin and PLA–gelatin coaxial fibers characterized by a thick sheath layer were

380 and 393 mmHg, respectively, while PU–gelatin scaffolds composed of fibers with a thin sheath layer exhibited the highest average burst pressure of 540 mmHg. The hydrophobic core diameter of the coaxially electrospun fibers might influence the burst pressure. The burst strength of all graft scaffolds possesses adequate strength (~3–5 times the physiological pressure) for implantation. The interaction between the coaxial polymer layers led to a decrease in the burst pressure, when compared to the individual use of the hydrophobic core polymers. PCL grafts, for example, have been shown to exhibit a burst pressure in the range 650–2000 mmHg, while PLA grafts and PU grafts were in the range 800–2200 mmHg.[38–40] The significant decrease in the burst pressure, particularly in the cases of PCL–gelatin and PLA–gelatin scaffolds, might be due to their extremely high compliance, which leads to high strain deformation causing breaking of the cross-linking bonds under low pressures. Nevertheless, the scaffolds have sufficient strength for implantation, while the addition of a gelatin sheath in the nanofibers led to the reduction in brittleness and formation of a softer biomaterial.

3.7. Compliance of Tubular Vascular Scaffolds with Coaxially Structured Nanofibers

The average compliance values of the 3D vascular grafts with coaxially spun fibers are shown in Table 3. Figure 6 demonstrates the representative curves showing the percent of change in graft diameter with respect to increasing pressure. The compliance of the vascular grafts correlated well with the sheath thickness. The PCL–gelatin and PLA–gelatin scaffolds both showed high compliance with averages of 29.7 and 27.7%, respectively, while the PU–gelatin scaffold exhibited the least compliance of 7.9%. The compliance values are superior to many native vein grafts such as saphenous vein (~4.5%) and umbilical vein (~3.7%), and are higher than or similar to the compliance of elastic artery.[36] Compliance is an important parameter in graft healing and vascular regeneration, largely due to the influence of hemodynamics at the site of anastomosis and subsequent responses from vascular cells to hemodynamics-induced changes in the shear stress and circumferential stretch.[22,37] A highly compliant vascular graft, with the compliance and thus mechanical deformation matching the native arteries, promises to significantly improve graft patency and vascular tissue regeneration.

3.8. In Vitro Cell Biocompatibility on the Vascular Scaffolds with Coaxially Structured Nanofibers

MTT assay results showing vascular cell proliferation on coaxially structured nanofibers are depicted in Figure 7. Fluorescent microscopy images show cell morphology of hSMCs and hECs on coaxially electrospun scaffolds (Figure 8). All coaxially electrospun scaffolds supported the sandwiched coculture with hECs on one side of the scaffolds and hSMCs on the other, suggesting the nutrient transport through the scaffolding membranes to maintain cell viability and growth. The cell morphology and proliferation of both hECs and hSMCs were determined after 6 days of cell culture. Both hECs and hSMCs on the PCL–gelatin scaffold showed the highest cell growth reaching confluency, when compared to PU–gelatin and PLA–gelatin scaffolds, suggesting the suitability of PCL–gelatin for vascular cell coculture. Though the nanofibers of all the scaffolds present gelatin on their surfaces for cell recognition and interaction, the fact that the highest cell growth was found on the PCL–gelatin coaxially structured nanofibers suggests that cell growth might be affected by the

thickness of the sheath.. The recognition sites in gelatin, a denatured form of collagen, aid in specific cell–scaffold interactions and support cell growth, providing biomimetic microenvironments for adhesion and function of hECs and hSMCs and preventing hSMC overgrowth. However, the hydrophilicity and the presence of cell recognition sites of gelatin significantly decreases with genipin cross-linking which consumes the active groups in gelatin. As shown by the swelling properties of the three scaffolds, the cross-linked PCL–gelatin scaffold possessed the highest swelling property, suggesting that its thick gelatin layer retained the highest amount of active groups in gelatin which might assist to promote cell adhesion and growth. In addition, the higher water content in the PCL–gelatin scaffold facilitates better transportation of nutrients and metabolic wastes when compared to the others. The porous structure with proper softness might also increase the probability of cell penetration after degradation of gelatin on the surface. Since the nanofibrous scaffolds have pores of dimensions that are much smaller than the normal cell size of 10 μm, it may inhibit cell migration. The dynamic architecture of the fibers with a more readily degradable gelatin sheath could also allow the cells to adjust according to the pore size and grow into the nanofiber matrixes creating higher pore size and volume after gelatin degradation on the surface.[41] The high growth rate of vascular cells simultaneously on the PCL–gelatin scaffolds exhibits its high potential as a biodegradable vascular scaffold for regeneration.

4. CONCLUSION

We have developed three types of coaxially electrospun 3D nanofibrous vascular scaffolds, using the mixtures of polymer solutions with a fixed ratio of 1:5 between a hydrophobic, synthetic, biodegradable polymer (PU, PCL, or PLA) and a hydrophilic, naturally derived gelatin. The hybrid nanofibers demonstrate a highly interactive, multilayered structure showing a hydrophobic core, a gelatin sheath, and an interactive layer. Varied interactions between the core and the sheath materials lead to the difference in the sheath thickness, core–sheath structure, and consequently water swelling ratio of scaffolds, mechanical stiffness and strength, tubular graft compliance, and growth of cocultured vascular cells on scaffolds. Inclusion of gelatin as a nanofiber sheath greatly improved scaffold elasticity, led to the formation of highly compliant tubular grafts, and provided high water content preventing fluid from leaking out of the graft under normal blood pressure while ensuring the transport of nutrients and signaling molecules. The scaffolds also exhibited excellent thermal stability for vascular tissue engineering applications. Among the three types of scaffolds, nanofibers in PCL–gelatin scaffolds exhibit the thickest gelatin sheath, strongest core–sheath interactions, and highest swelling ratio, demonstrating as the most compliant graft and best supporting both hEC and hSMC growth; thereby, it shows great potential for vascular graft construction. Future studies will focus on tuning graft compliance by adjusting the concentration ratio and structure of hybrid nanofibers in the graft scaffolds to meet the needs of replacing a wide range of arteries in various clinical settings.

Acknowledgments

We sincerely acknowledge Ms. Dorothy Dill in the Anschutz Medical Campus of the University of Colorado at Denver for her assistance with transmission electron microscopy. The research is funded by NIH (NHLBI 119371 to W.T.).

REFERENCES

1. Liu H, Li X, Zhou G, Fan H, Fan Y. Electrospun sulfated silk fibroin nanofibrous scaffolds for vascular tissue engineering. Biomaterials. 2011; 32:3784–3793. [PubMed: 21376391]
2. Wang P, Liu J, Zhang T. In Vitro Biocompatibility of Electrospun Chitosan/Collagen Scaffold. J. Nanomater. 2013; 2013(958172)
3. Williamson M, Black R, Kielty K. PCL–PU composite vascular scaffold production for vascular tissue engineering: Attachment, proliferation and bioactivity of human vascular endothelial cells. Biomaterials. 2006; 27:3608–3616. [PubMed: 16530824]
4. Wu X-M, Branford-White CJ, Yu D-G, Chatterton NP, Zhu L-M. Preparation of core-shell PAN nanofibers encapsulated α-tocopherol acetate and ascorbic acid 2-phosphate for photoprotection. Colloids Surf., B. 2011; 82:247–252.
5. Lee GH, Song J-C, Yoon K-B. Controlled wall thickness and porosity of polymeric hollow nanofibers by coaxial electrospinning. Macromol. Res. 2010; 18:571–576.
6. Yarin AL. Coaxial electrospinning and emulsion electrospinning of core-shell fibers. Polym. Adv. Technol. 2001; 22:310–317.
7. Reznik SN, Yarin AL, Zussman E, Bercovici L. Evolution of a compound droplet attached to a core shell nozzle under the action of a strong electric field. Phys. Fluids. 2006; 18:1–13.
8. Reneker DH, Yarin AL. Electrospinning jets and polymer nanofibers. Polymer. 2008; 49:2387–2425.
9. Zhang Y, Ouyang H, Lim CT, Ramakrishna S, Huang Z-M. Electrospinning of gelatin fibers and gelatin/PCL composite fibrous scaffolds. J. Biomed. Mater. Res. 2005; 72B:156–165.
10. Nagiah N, Madhavi L, Anitha R, Srinivasan NT, Sivagnanam UT. Electrospinning of poly (3-hydroxybutyric acid) and gelatin blended thin films: Fabrication, characterization and application in skin regeneration. Polym. Bull. 2013; 70:2337–2358.
11. Nagiah N, Madhavi L, Anitha R, Anandan C, Srinivasan NT, Sivagnanam UT. Coaxially electrospun gelatin coated poly (3-hydroxybutyric acid) thin films for skin regeneration. Mater. Sci. Eng., C. 2013; 33:4444–4452.
12. Arumuganathar S, Irvine S, McEwan JR, Jayasinghe SN. A Novel Direct Aerodynamically Assisted Threading Methodology for Generating Biologically Viable Microthreads Encapsulating Living Primary Cells. J. Appl. Polym. Sci. 2008; 107:1215–1225.
13. Jia X, Zhao X, Li P, Zhang H, Huang J, Li H, Fan J, Feng W, Yuan X, Fan Y. Sustained Release of VEGF by Coaxial Electrospun Dextran/PLGA Fibrous Membranes in Vascular Tissue Engineering. J. Biomater. Sci., Polym. Ed. 2011; 22:1811–1827. [PubMed: 20961491]
14. Zhai W, Qiu L-j, Mo X-m, Wang S, Xu Y-f, Peng B, Liu M, Huang J-h, Wang G-c, Zheng J-h. Coaxial electrospinning of P(LLA-CL)/heparin biodegradable polymer nanofibers: potential vascular graft for substitution of femoral artery. J. Biomed. Mater. Res., Part B. 2013; 102:203–214.
15. Zhang H, Jia X, Han F, Zhao J, Zhao Y, Fan Y, Yuan X. Dual-delivery of VEGF and PDGF by double-layered electrospun membranes for blood vessel regeneration. Biomaterials. 2013; 34:2202–2212. [PubMed: 23290468]
16. Wen X, Hong Z, Xiao-Yan Y. Ultrafine Fibrous Membranes by Coaxial Electrospinning for Artificial Blood Vessel. Chem. J. Chin. Univ. 2011; 32:1396–1400.
17. Wang T, Ji X, Jin L, Feng Z, Wu J, Zheng J, Wang H, Xu Z, Guo L, He N. Fabrication and Characterization of Heparin-Grafted Poly-l-lactic acid–Chitosan Core–Shell Nanofibers Scaffold for Vascular Gasket. ACS Appl. Mater. Interfaces. 2013; 5:3757–3763. [PubMed: 23586670]
18. Zeng J, Xu X, Chen X, Liang Q, Bian X, Yang L, Jing X. Biodegradable electrospun fibers for drug delivery. J. Controlled Release. 2003; 92:227–231.
19. Fu W, Liu Z, Feng B, Hu R, He X, Wang H, Yin M, Huang H, Zhang H, Wang W. Electrospun gelatin/PCL and collagen/PLCL scaffolds for vascular tissue engineering. Int. J. Nanomed. 2014; 9:2335–2344.
20. Zhu C, Ma X, Xian L, Zhou Y, Fan D. Characterization of a co-electrospun scaffold of HLC/CS/PLA for vascular tissue engineering. Biomed Mater. Eng. 2014; 24:1999–2005. [PubMed: 25226896]

21. Jia L, Prabhakaran M, Qin X, Kai D, Ramakrishna S. Biocompatibility evaluation of protein-incorporated electrospun polyurethane-based scaffolds with smooth muscle cells for vascular tissue engineering. J. Mater. Sci. 2013; 48:5113–5124.
22. Zilla P, Bezuidenhout D, Human P. Prosthetic vascular grafts: Wrong models, wrong questions and no healing. Biomaterials. 2007; 28:5009–5027. [PubMed: 17688939]
23. Zeugolis D, Khew S, Yew E, Ekaputra A, Tong Y, Yung L, Hutmacher D, Sheppard C, Raghunath M. Electro-spinning of pure collagen nano-fibres – Just an expensive way to make gelatin? Biomaterials. 2008; 29:2293–2305. [PubMed: 18313748]
24. Nguyen T-H, Lee B-T. Fabrication and characterization of cross-linked gelatin electro-spun nano-fibers. J. Biomed. Sci. Eng. 2010; 3:1117–1124.
25. Han J, Li M, Lelkes PI. Co-electrospun blends of PLGA, gelatin and elastin as anti-thrombogenic scaffolds for vascular grafts. 8th World Biomaterials Congress. 2008:2.
26. Panzavolta S, Gioffrè M, Focarete M, Gualandi C, Foroni L, Bigi A. Electrospun gelatin nanofibers: Optimization of genipin cross-linking to preserve fiber morphology after exposure to water. Acta Biomater. 2011; 7:1702–1709. [PubMed: 21095244]
27. Elzein T, Nasser-Eddine M, Delaite C, Bistac S, Dumas P. FTIR study of polycaprolactone chain organization at interfaces. J. Colloid Interface Sci. 2004; 273:381–387. [PubMed: 15082371]
28. Wang DK, Varanasi S, Fredericks PM, Hill DJT, Symons AL, Whittaker AK, Rasoul F. FT-IR characterization and hydrolysis of PLA–PEG-PLA based copolyester hydrogels with short PLA segments and a cytocompatibility study. J. Polym. Sci., Part A: Polym. Chem. 2013; 51:5163–5176.
29. Spagnuolo M, Lingyun L. Fabrication and Degradation of Electrospun Scaffolds from L-Tyrosine-Based Polyurethane Blends for Tissue Engineering Applications. ISRN Nanotechnology. 2012 Article ID 627420.
30. Naveen N, Kumar R, Balaji S, Uma TS, Natrajan TS, Sehgal PK. Synthesis of Nonwoven Nanofibers by Electrospinning – A Promising Biomaterial for Tissue Engineering and Drug Delivery. Adv. Eng. Mater. 2010; 12:B380–B387.
31. Muyonga JH, Cole B, Duodu KG. Fourier transform infrared (FTIR) spectroscopic study of acid soluble collagen and gelatin from skins and bones of young and adult Nile perch (Lates niloticus). Food Chem. 2004; 86:325–332.
32. Hashim DM, Man YBC, Norakasha R, Shuhaimi M, Salmah Y, Syahariza ZA. Potential use of Fourier transform infrared spectroscopy for differentiation of bovine and porcine gelatins. Food Chem. 2010; 118:856–860.
33. Vroman I, Tighzert L. Biodegradable Polymers. Materials. 2009; 2:307–344.
34. Shalumon KT, Anulekha KH, Girish CM, Prasanth R, Nair SV, Jayakumar R. Single step electrospinning of chitosan/poly(caprolactone) nanofibers using formic acid/acetone solvent mixture. Carbohydrate. Carbohydr. Polym. 2010; 80:413–419.
35. Sencadas V, Costa CM, Botelho G, Caparrós C, Ribeiro C, Gómez-Ribelles JL, Lanceros-Mendeza S. Thermal Properties of Electrospun Poly(Lactic Acid) Membranes. J. Macromol. Sci., Part B. Phys. 2012; 51:411–424.
36. Sarkar S, Salacinski HJ, Hamilton G, Seifalian AM. The Mechanical Properties of Infrainguinal Vascular Bypass Grafts: Their Role in Influencing Patency. Euro J. Vas Endovas Surg. 2006; 31:627–636.
37. Madhavan K, Elliott WH, Bonani W, Monnet E, Tan W. Mechanical and biocompatible characterizations of a readily available multilayer vascular graft. J. Biomed. Mater. Res., Part B. 2013; 101B:506–519.
38. Nezarati RM, Eifert MB, Dempsey DK, Cosgriff-Hernandez E. Electrospun vascular grafts with improved compliance matching to native vessels. J. Biomed. Mater. Res., Part B. 2015; 103:313–323.
39. Wang S, Zhang Y, Yin G, Wang H, Dong Z. Electrospun polylactide/silk fibroin–gelatin composite tubular scaffolds for small-diameter tissue engineering blood vessels. J. Appl. Polym. Sci. 2009; 113:2675–2682.
40. Drilling S, Gaumer J, Lannutti J. Fabrication of burst pressure competent vascular grafts via electrospinning: effects of microstructure. J. Biomed. Mater. Res., Part A. 2009; 88:923–934.

41. Rose JB, Pacelli S, Haj A, Dua HS, Hopkinson A, White LJ, Rose F. Gelatin based materials in ocular tissue engineering. Materials. 2014; 7:3106–3135.

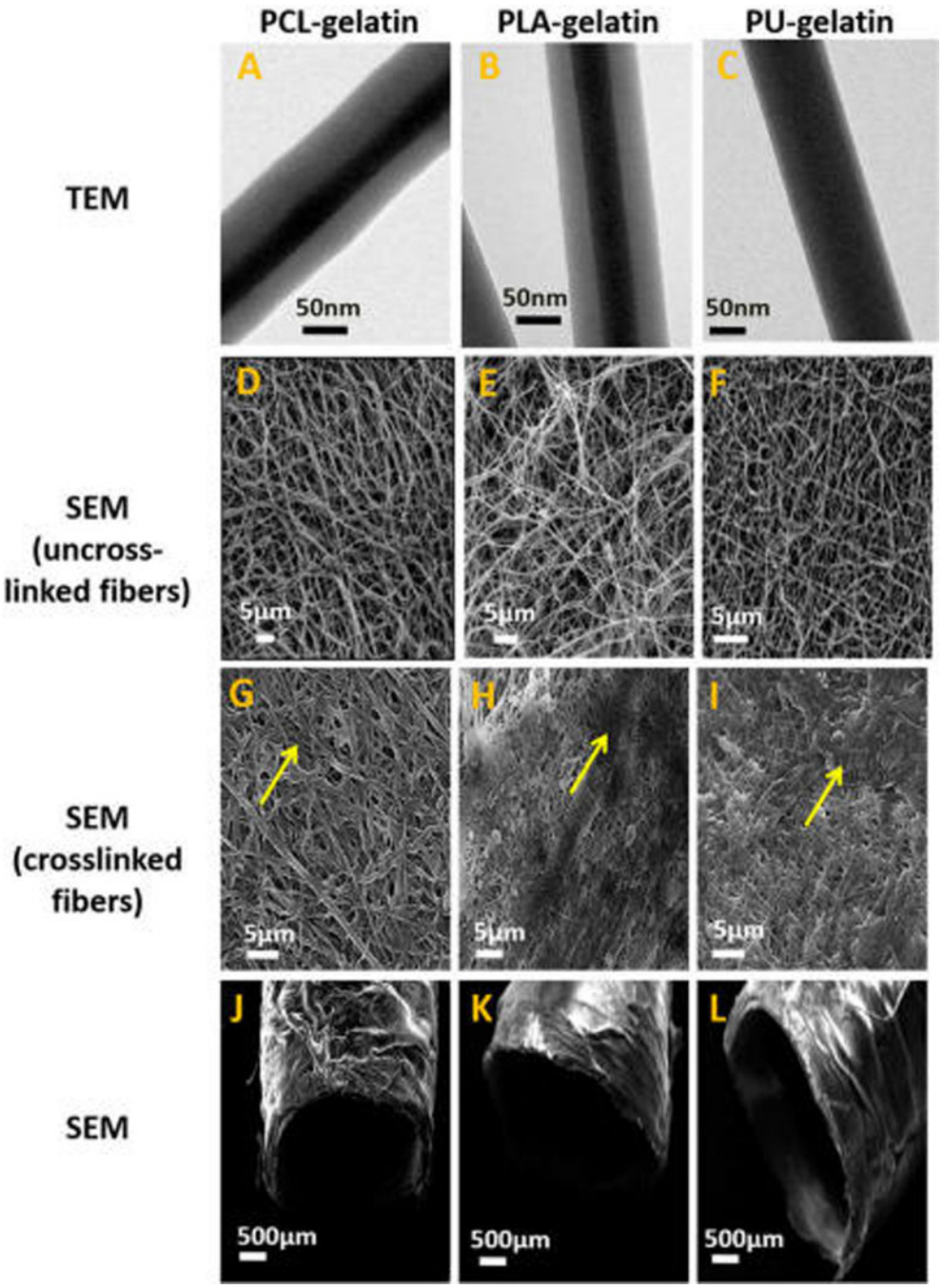

Figure 1.

TEM and SEM images of the graft scaffolds with coaxially spun nanofibers of PCL–gelatin (A, D, G, J), PLA–gelatin (B, E, H, K), and PU–gelatin (C, F, I, L) in their un-cross-linked (A–F) or cross-linked (G–L) states. Arrows point to the coalescence of the fibers.

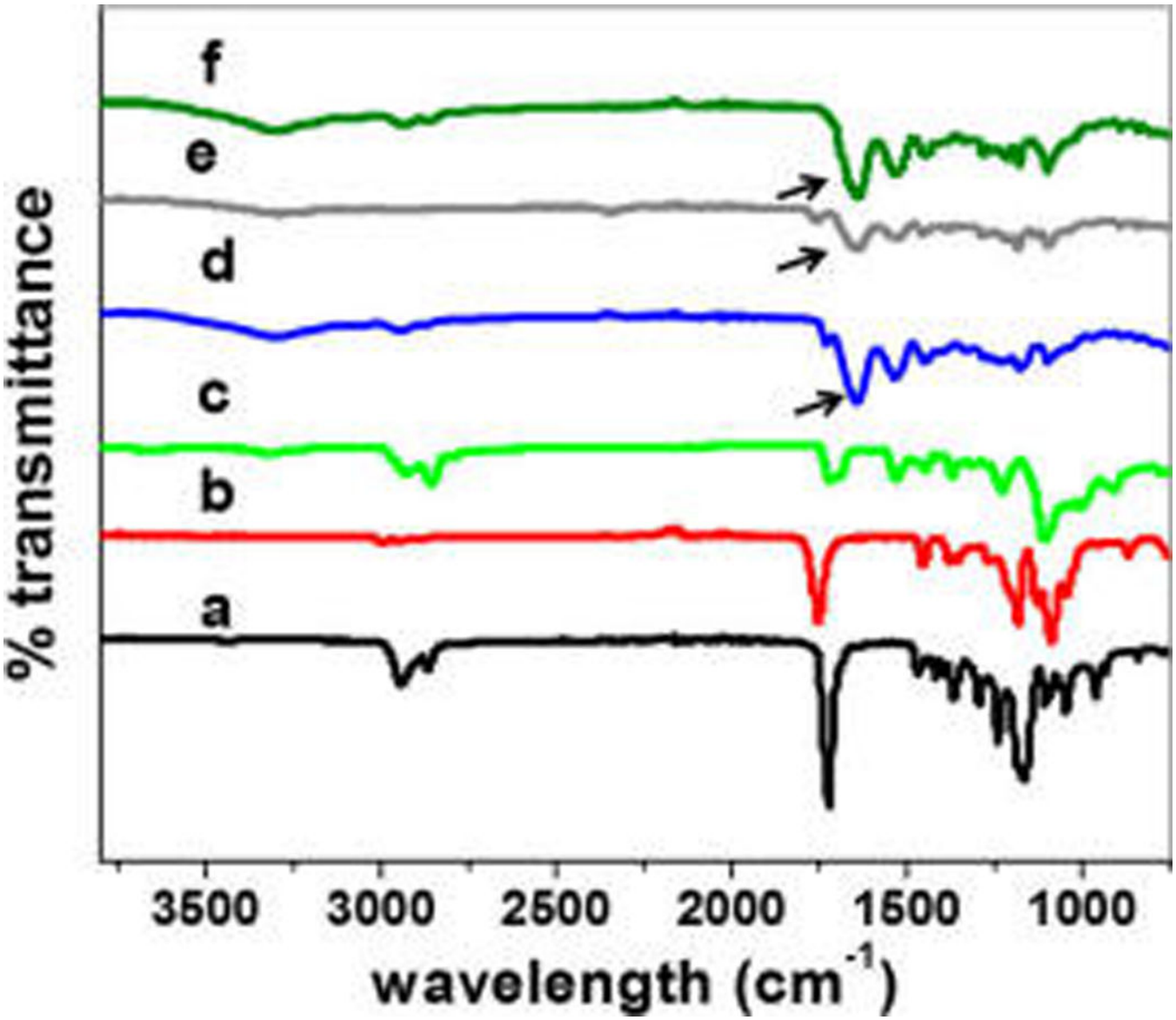

Figure 2.
ATR-FTIR spectra of electrospun fibers composed of PCL (a), PLA (b), and PU (c), as well as coaxially spun fibers of PCL–gelatin (d), PLA–gelatin (e), and PU–gelatin (f).

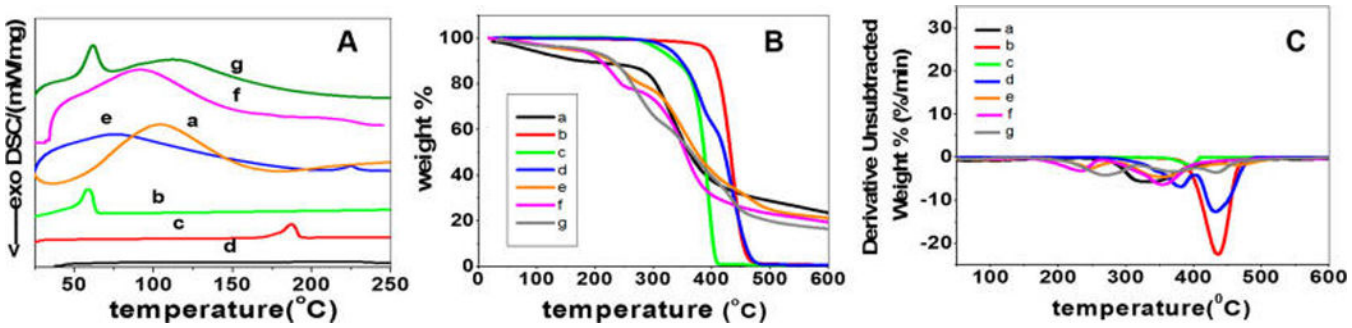

Figure 3.

Results from DSC (A), TGA (B), and DTA (C) measurements of individual polymers and their coaxially spun fibers: (a) gelatin, (b) PCL, (c) PLA, (d) PU, (e) PU–gelatin, (f) PLA–gelatin, and (g) PCL–gelatin.

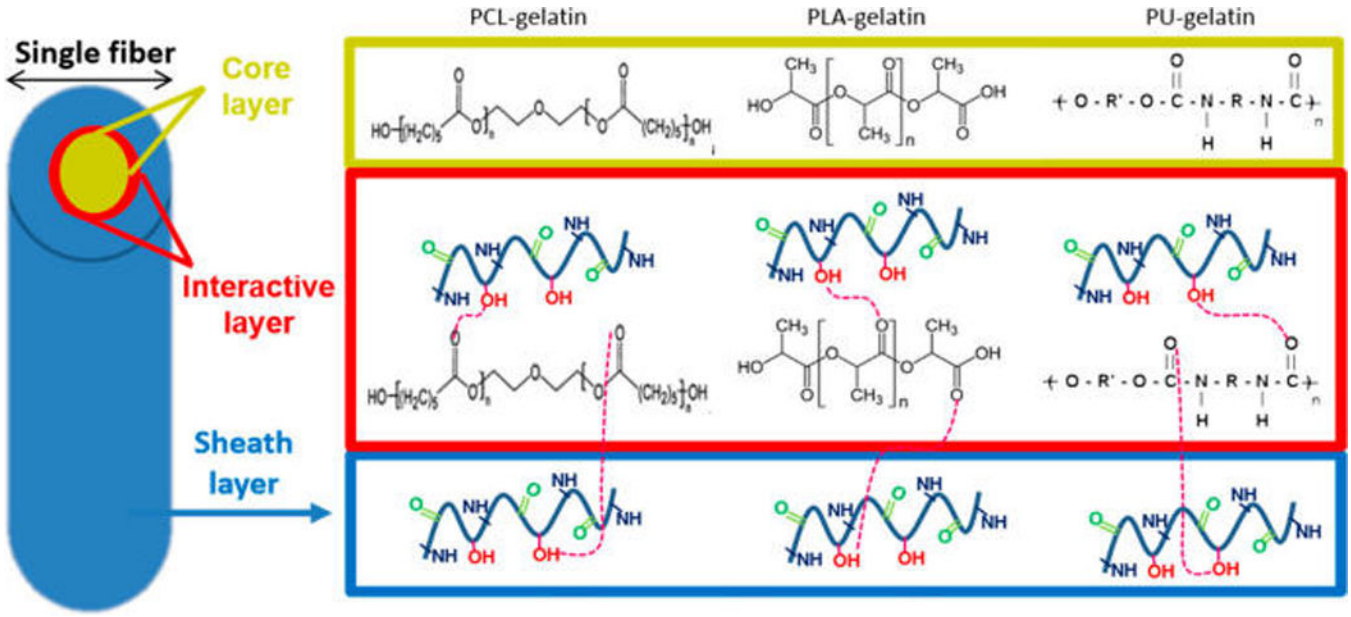

Figure 4.
Schematic representation of the interactions between sheath and core layers in the coaxially electrospun nanofibrous system.

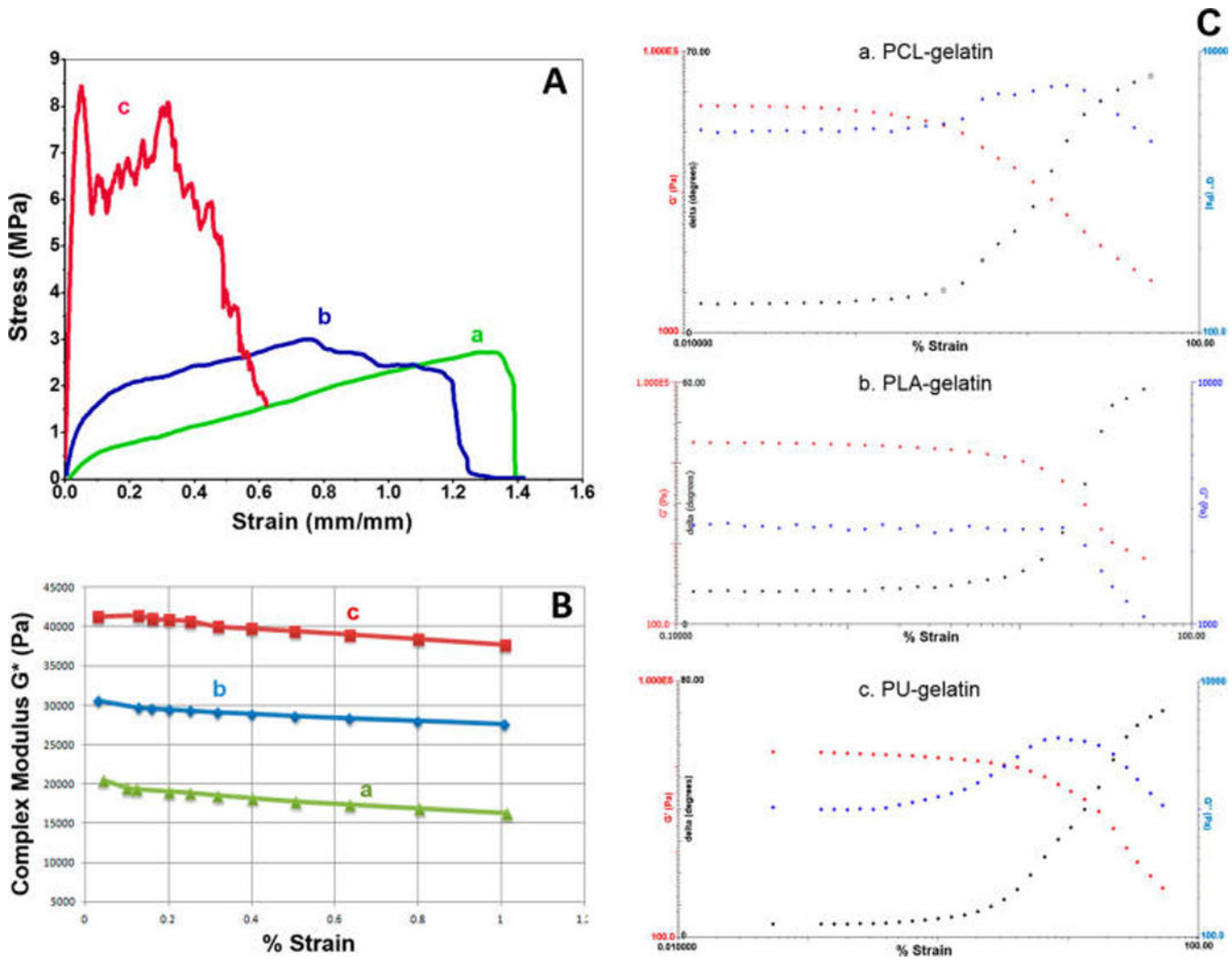

Figure 5.

Mechanical property measurements of scaffolds with coaxially spun fibers of PCL–gelatin (a), PLA–gelatin (b), and PU–gelatin (c). (A) Representative results from uniaxial tensile tests. (B) Results of complex modulus (G^*) in LVR as a function of strain. (C) Representative strain sweep results of G', G'', and tan δ showing viscoelastic properties of three fibrous scaffolds.

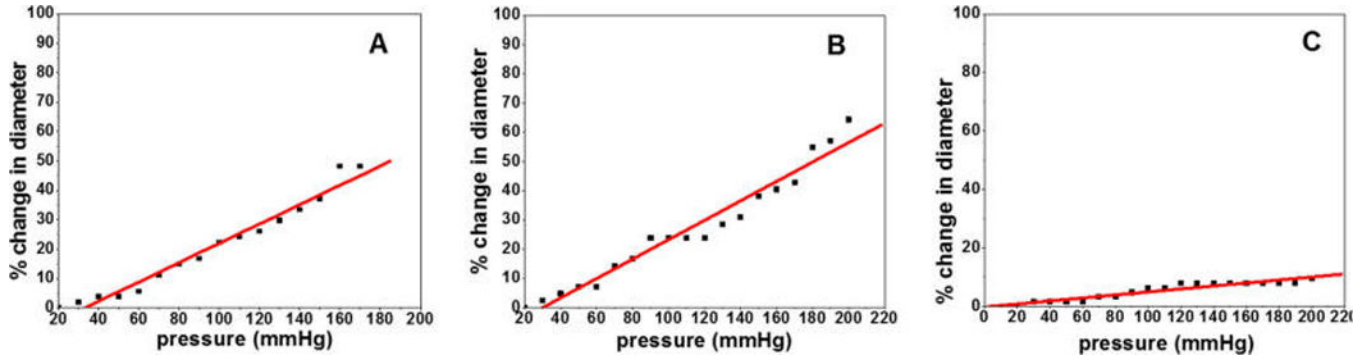

Figure 6.
Compliance of the scaffolds consisting of coaxially spun fibers of PCL–gelatin (A), PLA–gelatin (B), and PU–gelatin (C).

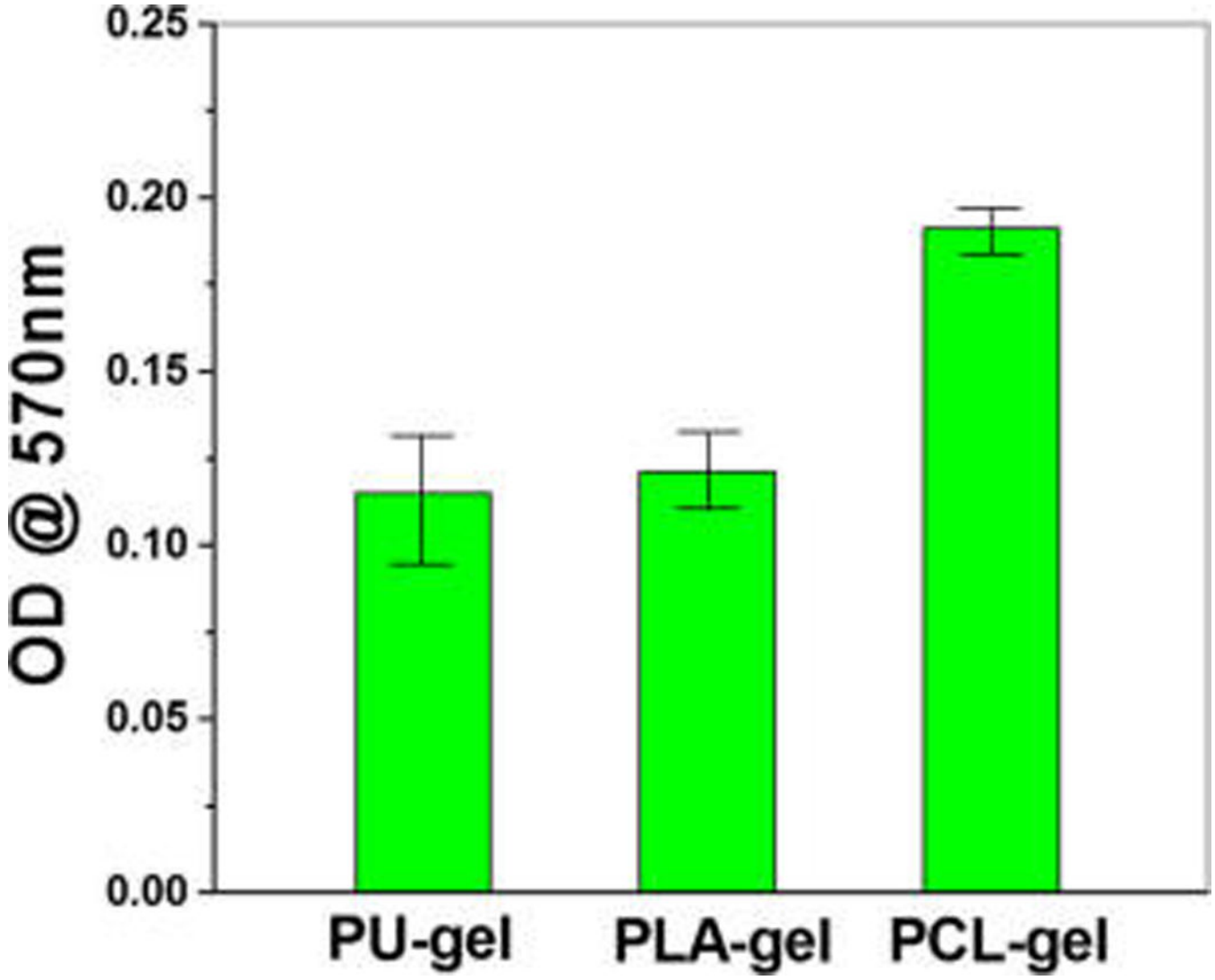

Figure 7.
MTT assay showing growth of vascular cell cocultures on the coaxially spun fibrous scaffolds.

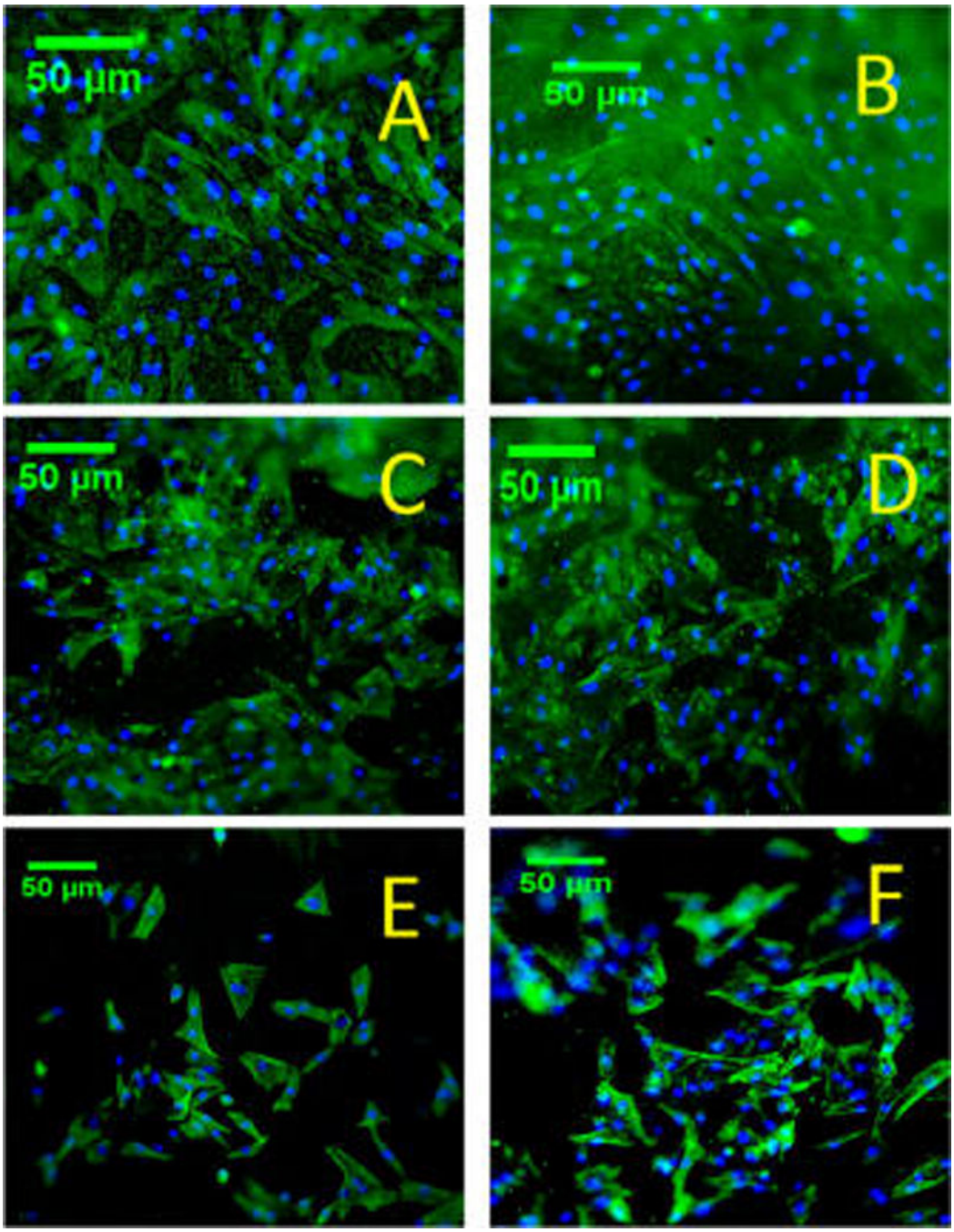

Figure 8.
Fluorescent microscopy images showing F-actin and DAPI stains in hECs (A, C, E) or hSMCs (B, D, F) cocultured on coaxially spun scaffolds composed of PCL–gelatin (A, B), PLA–gelatin (C, D), or PU–gelatin (E, F).

Table 1

ATR-FTIR Peaks of Individually or Coaxially Spun Fibers

wavelength (cm^{-1})	designation
1700–1750	C═O stretching
1226–1280	O—C—O stretching
1636–1640	C—O stretching of amide I in gelatin
1542–1548	N—H and C—H stretching in amide II
2900–3450	amide A of gelatin

Table 2

Thermal Properties of Individual Polymers and Coaxial Fibers

	coaxial PCL–gelatin	coaxial PLA–gelatin	coaxial PU-gelatin	gelatin	PCL	PLA	PU
T_{max1} (°C)	268.87	234.82	247.11	331.33	436.03	396.99	381.63
T_{max2} (°C)	369.47	354.5	355.91				432.32
T_{max3} (°C)	436.03		467.39				
$T_{-5\%}$ (°C)	192.69	153.38	178.17	85.59	395.99	308.66	330.64
transition temperature (°C)				105.3			
melting temperature (°C)	61.6	92.9	75.8		58.1	187.3	

Table 3

Physico-Mechanical and Graft Functional Properties of Coaxially Spun Scaffolds

	PCL–gelatin nanofibrous system	**PLA–gelatin nanofibrous system**	**PU–gelatin nanofibrous system**
average fiber diameter (nm)	330 ± 70	270 ± 90	210 ± 70
average swelling (%)	202 ± 26	168 ± 24	94 ± 30
average water permeability at 120 mmHg ($mL/cm^2/min$)	0	0	0
average burst pressure (mmHg)	380 ± 180	393 ± 140	540 ± 140
average compliance (% per 100 mmHg)	29.7 + 10.3	27.7 ± 7.6	7.9 ± 1.8
average suture retention (N)	4.33 ± 0.84	3.18 ± 1.12	2.35 ± 0.92
average elastic modulus (MPa)	5.98 ± 0.53	13.38 ± 3.18	70.01 ± 35.83
average storage modulus, G′ (KPa)	18 ± 9	28.7 ± 16	39.7 ± 20
average loss modulus, G″ (KPa)	2.8 ± 2	4.5 ± 3	5.7 ± 4
average shear stress (MPa)	1.72 ± 0.28	2.42 ± 0.46	3.93 ± 0.34